Dynamic Study of Homoleptic Bimetallic Platinum(II) Complexes Bridged by Fluorinated Benzenethiolates

Guillermina Rivera,[†] Sylvain Bernès,[‡] Cecilia Rodriguez de Barbarin,[§] and Hugo Torrens*[,†]

DEPg., F. Química, UNAM, Ciudad Universitaria, 04510 México D.F., Mexico, Centro de Química, IC-UAP, Blvd. 14 Sur 6303, San Manuel, 72570 Puebla Pue., Mexico, and F. Ciencias Químicas, UANL, Ciudad Universitaria, 66451 S. Nicolas de los Garza, Nuevo Leon, Mexico

Received April 6, 2001

A variable-temperature ^{19}F NMR study of the homoleptic bimetallic anionic complexes $X_2[Pt_2(\mu\text{-}SC_6F_5)_2(SC_6F_5)_4]$ ($X = K^+$, **1a**; Bu_4N^+, **1b**), $X_2[Pt_2(\mu\text{-}p\text{-}SC_6HF_4)_2(p\text{-}SC_6HF_4)_4]$ ($X = K^+$, **2a**; Bu_4N^+, **2b**), and $X_2[Pt_2(\mu\text{-}p\text{-}SC_6F_4(CF_3))_2(p\text{-}SC_6F_4(CF_3))_4]$ ($X = K^+$, **3a**; Bu_4N^+, **3b**) demonstrates the occurrence of dynamic processes that give rise to several stereoisomeric species in solution. Experimental evidence suggests that both inversion of configuration at the sulfur bridging atoms and hindered rotation about the carbon−sulfur bond are involved in generating the observed isomers. The solid-state X-ray diffraction structures of compounds **1b**, **2b**, and **3b** show that all three complexes contain planar $[Pt_2(\mu\text{-}S)_2]$ rings with an anti configuration.

Introduction

Binuclear complexes of d^8 transition metal ions of the type $[M_2(\mu\text{-}SR)_2(L)_4]$ display a variety of molecular conformations. The particular molecular conformation depends on a number of factors, such as whether the complexes incorporate a bent or a planar $[M_2(\mu\text{-}S)_2]$ ring,[1] the relative orientation of the substituents (R) at the sulfur bridging atoms,[2] and the extent of hindered rotation about the R−sulfur bond.[3]

Conversion between each of these isomers is accomplished either by flipping of the $[M_2(\mu\text{-}S)_2]$ ring,[4] hindered rotation about the R−sulfur bond,[5] inversion of configuration at tricoordinated pyramidal sulfur atoms,[6,7] or a combination these processes.[2]

Theoretical and experimental studies have shown that the energy differences between planar and bent structures are relatively small (ca. 40 kJ mol^{-1}), and it has been pointed out that, in some cases, the steric repulsion between terminal ligands or packing forces can ultimately affect the structural choice.[8]

On the other hand, variable-temperature NMR studies of complexes bearing pentafluorothiophenolate rings have shown that, as one would expect, C−S bond rotation is frequently restricted. The activation energies associated with this process are in the range 30−50 kJ mol^{-1}, and these values are larger than those found for comparable nonfluorinated compounds.[9−11]

X-ray diffraction studies have shown that solid-state interactions between fluorine atoms on neighboring groups could be responsible for the restriction of the C−S bond rotation.[12−14]

Inversion of configuration at metal-bridging sulfur atoms has been examined, and it was found that the activation energy involved in this process is in the range 40−80 kJ mol^{-1}.[15,16]

The binuclear complexes $K_2[Pt_2(\mu\text{-}SC_6F_5)_2(SC_6F_5)_4]^{2-}$ **1a** and $K_2[Pt_2(\mu\text{-}p\text{-}SC_6HF_4)_2(p\text{-}SC_6HF_4)_4]^{2-}$ **2a** have been reported previously.[17] In these studies the existence of isomers in solution was noted and attributed to sulfur inversion, although this phenomenon was not studied in greater depth.[17,18]

In this paper we report the synthesis of the new perfluorinated compounds $X_2[Pt_2(\mu\text{-}p\text{-}SC_6F_4(CF_3))_2(p\text{-}SC_6F_4(CF_3))_4]^{2-}$ ($X = K^+$, **3a**; $X = Bu_4N^+$, **3b**) as well as the variable-temperature ^{19}F NMR study and the crystal and molecular structures of $(Bu_4N)_2[Pt_2(\mu\text{-}SC_6F_5)_2(SC_6F_5)_4]$ **1b**, $(Bu_4N)_2[Pt_2(\mu\text{-}p\text{-}SC_6HF_4)_2(p\text{-}SC_6HF_4)_4]$ **2b**, and $(Bu_4N)_2[Pt_2(\mu\text{-}p\text{-}SC_6F_4(CF_3))_2(p\text{-}SC_6F_4(CF_3))_4]$ **3b**.

Experimental Section

All manipulations were carried out under dry oxygen-free dinitrogen atmospheres using Schlenk-tube techniques. Solvents were dried and degassed using standard techniques.[19] Thin-layer chromatography (TLC)

[†] UNAM, Ciudad Universitaria.
[‡] IC-UAP.
[§] UANL, Ciudad Universitaria.

(1) Aullón, G.; Ujaque, G.; Lledós, A.; Alvarez, S. *Chem. Eur. J.* **1999**, *5*, 1391−1410.
(2) Brown, M. D.; Puddephat, R. J.; Upton, C. E. E. *J. Chem. Soc., Dalton Trans.* **1976**, 2490−2494.
(3) Dixon, K. R.; Moss, K. C.; Smith, M. A. *J. Chem. Soc., Dalton Trans.* **1974**, 971−977.
(4) Dias, A. R.; Green, M. L. H. *J. Chem. Soc. A* **1971**, 1951−1956.
(5) Agh-Atabay, N. M.; Davidson, J. L. *J. Chem. Soc., Dalton Trans.* **1992**, 3531−3539.
(6) Abel, E. W.; Bush, R. P.; Hopton, F. J.; Jenkins, C. R. *Chem. Commun.* **1966**, 58−59.
(7) Haake, P.; Turley, P. C. *J. Am. Chem. Soc.* **1967**, *89*, 4611−4616.
(8) Aullón, G.; Ujaque, G.; Lledós, A.; Alvarez, S. *Inorg. Chem.* **1998**, *37*, 804−813.
(9) Meaking, P.; Ovenall, D. W.; Sheppard, W. A.; Jesson, J. P. *J. Am. Chem. Soc.* **1975**, *97*, 522−528.
(10) Wan Abu Bakar, W. A.; Davidson, J. L.; Lindsell, W. E.; McCullough, K. J. *J. Chem. Soc., Dalton Trans.* **1989**, 991−1001.
(11) Davidson, J. L.; McIntosh, C. H.; Leverd, P. C.; Lindsell, W. E.; Simpson, N. J. *J. Chem. Soc., Dalton Trans.* **1994**, 2423−2429.
(12) Arroyo, M.; Bernès, S.; Brianso, J. L.; Mayoral, E.; Richards, R. L.; Rius, J.; Torrens, H. *J. Organomet. Chem.* **2000**, *599*, 170−177.
(13) Wan Abu Bakar, W. A.; Davidson, J. L.; Lindsell, W. E.; McCullough, K. J. *J. Organomet. Chem.* **1987**, *322*, C1−C6.
(14) Castellanos, A.; Garcia, J. J.; Torrens, H.; Bailey, N.; Rodriguez de Barbarin, C. O.; Gutierrez, A.; del Rio, F. *J. Chem. Soc., Dalton Trans.* **1994**, 2861−2866.
(15) Shaver, A.; Morris, S.; Turrin, R.; Day, V. M. *Inorg. Chem.* **1990**, *29*, 3622−3623.
(16) Abel, E. W.; Bhargava, S. K.; Orrell, K. G. *Prog. Inorg. Chem.* **1984**, *32*, 1−118.
(17) Garcia, J.; Martín, E.; Morales, D.; Torrens, H. *Inorg. Chim. Acta* **1994**, *207*, 93−96.
(18) Usón, R.; Forniés, J.; Usón, M. A.; Apaolaza, J. A. *Inorg. Chim. Acta* **1991**, *187*, 175−180.
(19) Riddick, J. A.; Bunger, W. B.; Sakaro, T. K. *Organic Solvents: Physical Properties and Methods of Purification*, 4th ed.; Techniques of Chemistry, Volume II; Wiley-Interscience: New York, 1970.

10.1021/ic010437n CCC: $20.00
Published on Web 09/22/2001

Table 1. Crystallographic Data for Complexes **1b**, **2b**, and **3b**

complex	**1b**	**2b**	**3b**
chem formula	$C_{68}H_{72}F_{30}N_2Pt_2S_6$	$C_{68}H_{78}F_{24}N_2Pt_2S_6$	$C_{74}H_{72}F_{42}N_2Pt_2S_6$
fw	2069.82	1961.86	2369.88
space group	$P2_1/n$	$P2_1/n$	$P2_1/n$
a/Å	14.1703(17)	13.6707(8)	14.282(4)
b/Å	19.2766(18)	19.276(2)	22.526(4)
c/Å	14.763(3)	15.6448(15)	15.2241(19)
β/deg	94.362(11)	109.012(7)	90.406(18)
V/Å^3	4020.8(9)	3897.9(6)	4897.6(17)
Z	2	2	2
μ/mm^{-1}	3.741	3.843	3.099
ρ_{calcd}/(g cm^{-3})	1.709	1.672	1.607
temp/°C	25	25	25
λ/Å	0.71073	0.71073	0.71073
R indices ($I > 2\sigma(I)$)[a]	R1 = 4.11%, wR2 = 9.54%	R1 = 5.61%, wR2 = 14.56%	R1 = 7.21%, wR2 = 15.31%
R indices (all data)[a]	R1 = 6.28%, wR2 = 10.91%	R1 = 8.92%, wR2 = 17.03%	R1 = 15.98%, wR2 = 19.05%

[a] $R_{int} = \sum|F_o^2 - \langle F_o^2\rangle|/\sum F_o^2$, R1 = $\sum||F_o| - |F_c||/\sum|F_o|$, wR2 = $[\sum w(F_o^2 - F_c^2)^2/\sum w(F_o^2)^2]$, $S = [\sum w(F_o^2 - F_c^2)^2/(m - n)]$.

(Merck, 5 × 7.5 cm^2 Kiesegel 60 F_{254}) was used when possible to monitor the progress of the reaction under study.

Complexes were characterized by FTIR spectra recorded over the 4000−200 cm^{-1} range on a Perkin-Elmer 1600 spectrophotometer, and the samples were prepared as CsI pellets. Data are expressed in wavenumbers (cm^{-1}) with relative intensities (s = strong, m = medium, w = weak).

^{1}H and ^{19}F NMR spectra were measured with a Varian spectrometer operating at 299.7 and 282.0 MHz, respectively. ^{195}Pt NMR spectra were measured with a Bruker spectrometer operating at 64.5 MHz. Chemical shifts are relative to TMS [$\delta = 0$ (^{1}H)], $CFCl_3$ [$\delta = 0$ (^{19}F)] and $Na_2[PtCl_6]/D_2O$ [$\delta = 0$ (^{195}Pt)]. A standard variable-temperature unit was used to control the probe temperature, and this was checked periodically using a thermocouple to ensure that temperature readings were within ±1 °C. Complexes were dissolved in deuterated acetone.

Elemental analyses were determined by Galbraith Labs. Inc., USA.

$K_2[Pt_2(\mu\text{-}SC_6F_5)_2(SC_6F_5)_4]$ **1a**,[17] $K_2[Pt_2(\mu\text{-}p\text{-}SC_6HF_4)_2(p\text{-}SC_6HF_4)_4]$ **2a**,[17] and $[PtCl_2(COD)]$[20] were prepared according to the literature methods.

Pb(p-SC$_6$F$_4$(CF$_3$))$_2$. To a solution of $Pb(CH_3COO)_2$ (0.66 g, 2 mmol) in water (50 cm^3) was added H-p-$SC_6F_4(CF_3)$ (1.00 g, 4 mmol). A yellow precipitate formed, and this was filtered off and dried in vacuo to give $Pb(p\text{-}SC_6F_4(CF_3))_2$. The lead salt was recrystallized from acetone. Yield: 80%. Mp: 230 °C dec. $C_{14}F_{14}S_2Pb$: Anal. Calcd (%): C, 23.84; S, 9.09. Found (%): C, 23.8; S, 9.06. IR (cm^{-1}): 1642s, 1474vs, 1325vs, 1179vs, 1156vs, 1137vs, 977vs, 830vs, 715vs. ^{19}F NMR: δ −56.74 (pseudotriplet, p-CF_3), δ −133.57 (multiplet, o-F), δ −146.54 (multiplet, m-F).

K$_2$[Pt(p-SC$_6$F$_4$(CF$_3$))$_4$]. To a solution of KOH (0.27 g, 4.82 mmol) in water (10 cm^3) was added H-p-$SC_6F_4(CF_3)$ (1.21 g, 4.82 mmol), and the mixture was heated to 50 °C. After 30 min a solution of $K_2[PtCl_4]$ (0.5 g, 1.2 mmol) in water (10 cm^3) was added dropwise, and the mixture was stirred for 2 h. The solution was then filtered and the filtrate dried in vacuo to give $K_2[Pt(p\text{-}SC_6F_4(CF_3))_4]$ as a red solid. Yield: 74%. Mp: 240 °C dec. Anal. Calcd for $C_{28}F_{28}K_2PtS_4$ (%): C, 26.49; S, 10.1. Found (%): C, 26.4; S, 10.0. IR (cm^{-1}): 1644s, 1469vs, 1328vs, 1181s, 1139s, 969vs, 827s, 714s. ^{19}F NMR: δ −54.64 (pseudotriplet, p-CF_3), δ −130.98 (multiplet, o-F), δ −147.86 (multiplet, m-F).

[Pt(p-SC$_6$F$_4$(CF$_3$))$_2$(COD)]. To a suspension of $[PtCl_2(COD)]$ (0.10 g, 0.27 mmol) in acetone (25 cm^3) was added a solution of $Pb(p\text{-}SC_6F_4(CF_3))_2$ (0.19 g, 0.27 mmol) in acetone. A white solid precipitated from the resulting yellow solution, and this was filtered off and washed with acetone. The filtrate was evaporated to dryness under reduced pressure to afford pale yellow microcrystals of $[Pt(p\text{-}SC_6F_4(CF_3))_2(COD)]$. Yield: 93%. Mp: 247 °C dec. Anal. Calcd for $C_{22}H_{12}F_{14}PtS_2$ (%): C, 32.97; H, 1.51; S, 8.0. Found (%): C, 32.8; H, 1.5; S, 8.1. IR (cm^{-1}): 1643m, 1476vs, 1430m, 1386m, 1323vs, 1175s, 1144s, 976vs, 830s, 714s. ^{19}F NMR: δ −57.21 (pseudotriplet, p-CF_3), δ −132.06 (multiplet, o-F), δ −145.46 (multiplet, m-F).

K$_2$[Pt$_2$(μ-p-SC$_6$F$_4$(CF$_3$))$_2$(p-SC$_6$F$_4$(CF$_3$))$_4$] 3a. To a solution of $K_2[Pt(p\text{-}SC_6F_4(CF_3))_4]$ (0.10 g, 0.079 mmol) in acetone (25 cm^3) was added a solution of $[Pt(p\text{-}SC_6F_4(CF_3))_2COD]$ (0.06 g, 0.079 mmol) in acetone (25 cm^3). The reaction mixture was heated under reflux, and the course of the reaction was followed by thin-layer chromatography (TLC). After 63 h the solvent was distilled off under vacuum. The solid product was washed with benzene to give $K_2[Pt_2(\mu\text{-}p\text{-}SC_6F_4(CF_3))_2(p\text{-}SC_6F_4(CF_3))_4]$ **3a**. Yield: 86%. Mp: 245 °C dec. Anal. Calcd for $C_{42}F_{42}K_2Pt_2S_6$ (%): C, 26.76; S, 10.21. Found (%): C, 26.7; S, 10.1. IR (cm^{-1}): 1643m, 1475vs, 1178s, 1327vs, 976s, 828m, 715s.

(Bu$_4$N)$_2$[Pt$_2$(μ-p-SC$_6$F$_4$(CF$_3$))$_2$(p-SC$_6$F$_4$(CF$_3$))$_4$] 3b was obtained after treatment of **3a** with $(Bu_4N)Cl$ in acetone at room temperature. Yield: 91%. Mp: 119−120 °C. Anal. Calcd for $C_{74}H_{72}F_{42}N_2S_6Pt_2$ (%): C 37.51; H, 3.06; S, 8.12. Found (%): C, 37.4; H, 3.1; S, 8.2. IR (cm^{-1}): 2965m, 1641s, 1478vs, 1384m, 1324vs, 1177s, 1141vs, 977s, 826m, 714s.

Table 2. Selected Bond Lengths (Å) and Angles (deg) for **1b**[a]

Pt1−S3	2.3115(18)	Pt1−S2	2.2984(18)
Pt1−S1	2.3217(16)	Pt1−S1′	2.3164(16)
S1−C1	1.785(7)	S1−Pt1′	2.3164(16)
S2−C7	1.752(7)	S3−C13	1.760(7)
S3−Pt1−S2	89.43(7)	S3−Pt1−S1	90.78(6)
S2−Pt1−S1	173.37(6)	S3−Pt1−S1′	172.16(7)
S2−Pt1−S1′	97.52(6)	S1−Pt1−S1′	82.74(6)
C1−S1−Pt1	105.7(2)	C1−S1−Pt1′	109.5(2)
Pt1−S1−Pt1′	97.26(6)	C7−S2−Pt1	108.5(2)
C13−S3−Pt1	105.9(2)		

[a] Primed atoms are generated by inversion through a center of symmetry occupied by Pt1. For the Pt1 coordinates given in the Supporting Information for **1b**, the transformation to generate the primed atoms is $-x + 2, -y, -z$.

X-ray Diffraction Data. Suitable single crystals of complexes **1b**, **2b**, and **3b** were obtained by slow evaporation of solutions and were found to be stable in air. Pertinent crystal data and other crystallographic parameters are listed in Table 1. The diffraction data were collected at 295 K on a Bruker P4 diffractometer[21] using graphite-monochromated Mo Kα radiation ($\lambda = 0.71073$ Å) and a $\theta/2\theta$ or ω scan mode with variable scan speed. Absorption corrections were applied using ψ-scans.

For all three complexes the non-H atoms were refined anisotropically without restraints on thermal parameters, regardless of the disordered fragments. Structures were solved and refined using routine procedures.[22]

For the anion, due to the large atomic displacement parameters of the ligand C13···C18, the corresponding ring was refined as an idealized

(20) Drew, D.; Doyle, R. J. *Inorganic Synthesis*; Angelici, R. J., Ed.; J. Wiley & Sons: 1990; Vol. 28, p 346.

(21) Fait, J. *XSCANS Users Manual*; Siemens Analytical X-ray Instruments Inc.: Madison, WI, 1991.

(22) Sheldrick, G. M. *SHELX97 Users Manual*; University of Göttingen: Göttingen, Germany, 1997.

Table 3. Selected Bond Lengths (Å) and Angles (deg) for **2b**[a]

Pt1−S3	2.3012(17)	Pt1−S2	2.3141(16)
Pt1−S1	2.3174(16)	Pt1−S1′	2.3271(16)
S1−C1	1.774(5)	S1−Pt1′	2.3271(15)
S2−C7	1.731(6)	S3−C13	1.782(5)
S3−Pt1−S2	84.07(6)	S3−Pt1−S1	98.77(6)
S2−Pt1−S1	169.37(5)	S3−Pt1−S1′	173.59(5)
S2−Pt1−S1′	95.41(6)	S1−Pt1−S1′	82.91(6)
C1−S1−Pt1	110.3(2)	C1−S1−Pt1′	107.3(2)
Pt1−S1−Pt1′	97.09(6)	C7−S2−Pt1	111.6(2)
C13−S3−Pt1	108.77(17)		

[a] Primed atoms are generated by inversion through a center of symmetry occupied by Pt1. For the Pt1 coordinates given in the Supporting Information for **2b**, the transformation to generate the primed atoms is $-x + 1, -y + 2, -z + 2$.

hexagon and the four C−F bond lengths were restrained to 1.34(2) Å. Finally, in the case of **3b**, all terminal CF_3 groups are disordered, a situation that is common for this fragment. F73/F74 and F143/F144 were refined with occupation factors of 0.5, while F211/F212/F213 are disordered, as are F214/F215/F216, the occupation factors being 0.67 and 0.33, respectively.

Selected geometric parameters for **1b**, **2b**, and **3b** are listed in Tables 2, 3, and 4, respectively.

Results and Discussion

Complex anions **1**−**3** were prepared according to reactions 1 and 2:

$$K_2[Pt(SR)_4] + [Pt(SR)_2(COD)] \rightarrow K_2[Pt_2(\mu\text{-}SR)_2(SR)_4] + COD \quad (1)$$

R = C_6F_5 **1a**, *p*-C_6HF_4 **2a**, *p*-$C_6F_4(CF_3)$ **3a**; COD = 1,5-cyclooctadiene

$$K_2[Pt_2(\mu\text{-}SR)_2(SR)_4] + 2(N(C_4H_9)_4)Cl \rightarrow (N(C_4H_9)_4)_2[Pt_2(\mu\text{-}SR)_2(SR)_4] + 2KCl \quad (2)$$

R = C_6F_5 **1b**, *p*-C_6HF_4 **2b**, *p*-$C_6F_4(CF_3)$ **3b**

Reaction 1 suggests the possibility of preparing mixed complexes of the type $[Pt_2(\mu\text{-}SR')_2(SR)_4]$ ($R' \neq R$). However, the only products isolated after reacting $[Pt(SR)_2(COD)]$ and $K_2[Pt(SR')_4]$ were the corresponding homoleptic compounds $K_2[Pt_2(\mu\text{-}SR)_2(SR)_4]$ and $K_2[Pt_2(\mu\text{-}SR')_2(SR')_4]$ [R and R′ = C_6F_5, *p*-C_6HF_4, or *p*-$C_6F_4(CF_3)$], as shown in reaction 3. This fact indicates that ligand rearrangement is a highly favored process during this reaction.

$$3K_2[Pt(SR')_4] + 3[Pt(SR)_2(COD)] \rightarrow K_2[Pt_2(\mu\text{-}SR)_2(SR)_4] + 2K_2[Pt_2(\mu\text{-}SR')_2(SR')_4] + 3COD \quad (3)$$

R and R′ = C_6F_5, *p*-C_6HF_4, or *p*-$C_6F_4(CF_3)$; COD = 1,5-cyclooctadiene

Complexes **1**−**3** are yellow-orange crystalline solids that are relatively stable in air. Complexes **1a**, **2a**, and **3a** are soluble in acetone whereas compounds **1b**, **2b**, and **3b** are soluble in acetone, dichloromethane, chloroform, and ethanol.

Crystal and Molecular Structures of 1b, 2b, and 3b. The molecular structures of $(Bu_4N)_2[Pt_2(m\text{-}SC_6F_5)_2(SC_6F_5)_4]$ **1b**, $(Bu_4N)_2[Pt_2(m\text{-}p\text{-}SC_6HF_4)_2(p\text{-}SC_6HF_4)_4]$ **2b**, and $(Bu_4N)_2[Pt_2(m\text{-}p\text{-}SC_6F_4(CF_3))_2(p\text{-}SC_6F_4(CF_3))_4]$ **3b** are shown in Figures 1−3, respectively. Selected bond distances and angles are collected in Tables 2−4, respectively.

Table 4. Selected Bond Lengths (Å) and Angles (deg) for **3b**[a]

Pt1−S2	2.306(4)	Pt1−S1′	2.323(3)
Pt1−S3	2.325(4)	Pt1−S1	2.326(3)
S1−C1	1.776(14)	S1−Pt1′	2.323(3)
S2−C8	1.765(15)	S3−C15	1.759(14)
S2−Pt1−S1′	169.37(15)	S2−Pt1−S3	88.06(14)
S1′−Pt1−S3	91.74(13)	S2−Pt1−S1	98.75(14)
S1′−Pt1−S1	82.74(13)	S3−Pt1−S1	170.68(14)
C1−S1−Pt1′	107.6(5)	C1−S1−Pt1	111.4(5)
Pt1′−S1−Pt1	97.26(13)	C8−S2−Pt1	110.5(5)
C15−S3−Pt1	103.8(5)		

[a] Primed atoms are generated by inversion through a center of symmetry occupied by Pt1. For the Pt1 coordinates given in the Supporting Information for **3b**, the transformation to generate the primed atoms is $-x + 1, -y + 2, -z$.

Complex anions **1**−**3** were characterized by single-crystal X-ray diffraction of complexes containing the bulky cation Bu_4N^+. All complexes show the same space group, but they are not isomorphous (see Table 1). The asymmetric unit of the three structures contains one cation and one metal atom bonded to three thiolate ligands. This latter fragment lies close to an inversion center of space group $P2_1/n$, which yields a centrosymmetric dianion including a planar $[Pt_2(\mu\text{-}S)_2]$ skeleton (see Figures 1−3). Sulfur atoms of terminal thiolate ligands are located in the plane defined by the metallic core.

The most interesting structural feature is the configuration of the thiolate rings. The bridging ligand displays an anti configuration in all cases. However, the terminal ligands adopt a different configuration with respect to the bridging thiolates. For **1b** and **3b**, ligand S2 is almost parallel to the bridging ligand while ligand S3 is almost perpendicular to the bridge (see Figures 1 and 3). In complex **1b**, the angle between the mean planes of ligands S1 and S2 is 12.1° whereas the angle between planes S1 and S3 is 95° (mean planes are calculated through the six C atoms of the aromatic rings). In the case of anion **3b**, these angles are 2.5° and 92.5°, respectively. Unexpectedly, the configuration is different for **2b**, where *both* terminal ligands S2 and S3 are almost parallel to the bridging ligand (see Figure 2): the dihedral angles between the aromatic rings are 15.7° and 22.7° for the S1/S2 and S1/S3 moieties, respectively. In all cases the spatial arrangement of the thiolates does not allow strong intramolecular interactions between the aromatic groups.

In a search for intramolecular interactions that could restrict rotation of the thiophenolate ring (vide infra), we examined the nearest 12 Pt−F distances for the three anions. The shortest Pt···F distance found is 3.249 Å whereas the sum of van der Waals radii for Pt and F is ca. 3.22−3.3 Å.[23,24] These intramolecular interactions could, therefore, restrict the orientational freedom of the ligands. This situation may explain the fact that different configurations are observed for **1b** and **2b**, even though the ligands are very similar. The Pt···F interactions probably give rise to a relatively high energy barrier between one configuration and the other in the lattice, thus precluding the possibility of switching in the solid state. In the case of anion **1b**, diffraction data for three crystals obtained from three different attempts at crystallization resulted in the same configuration for the anion. These findings corroborate the idea that intramolecular interactions are important in stabilizing the observed configurations.

(23) Altomare, A.; Cascarno, G.; Giacovazzo, C.; Guagliardi, A.; Burla, M. C.; Polidori, G.; Camalli, M. *SIR97 Users Manual*; University of Bari: Bari, Italy, 1997.
(24) Bondi, A. *J. Phys. Chem.* **1964**, *68*, 441−444.

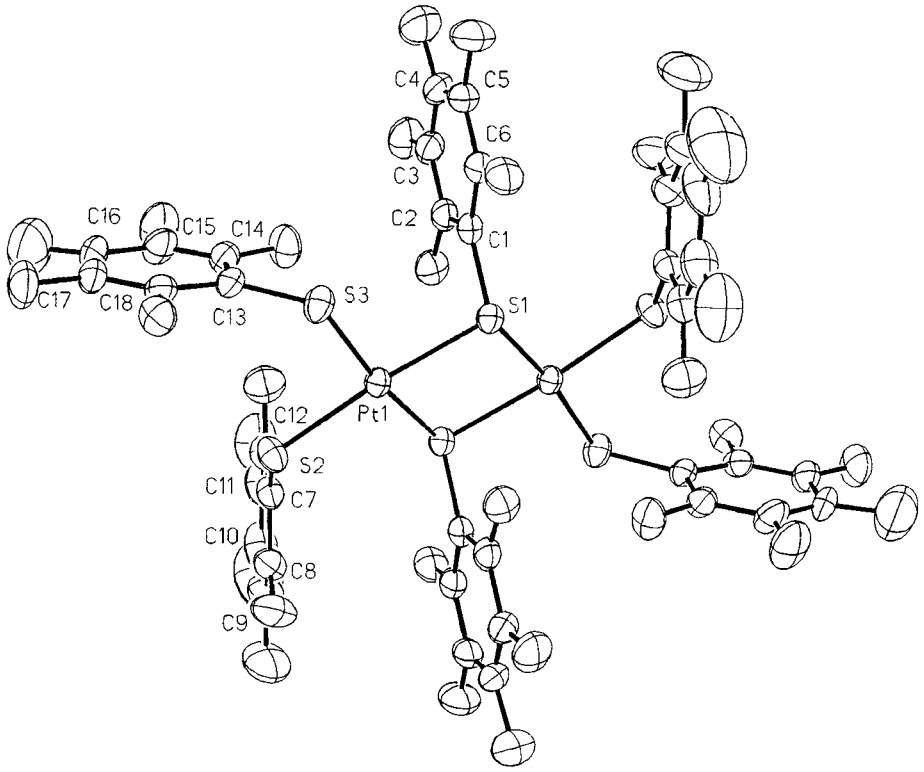

Figure 1. Structure of anion **1b** showing 20% probability displacement ellipsoids.

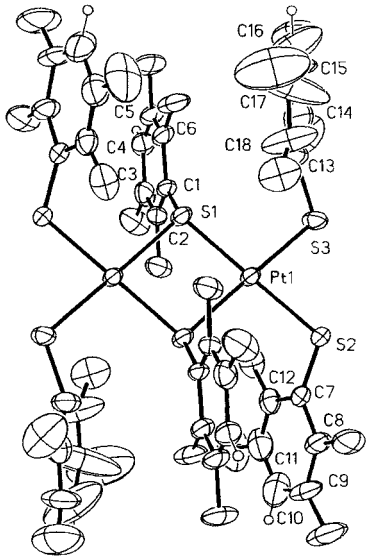

Figure 2. Structure of anion **2b** showing 20% probability displacement ellipsoids. Note the thermal agitation for ligand S3.

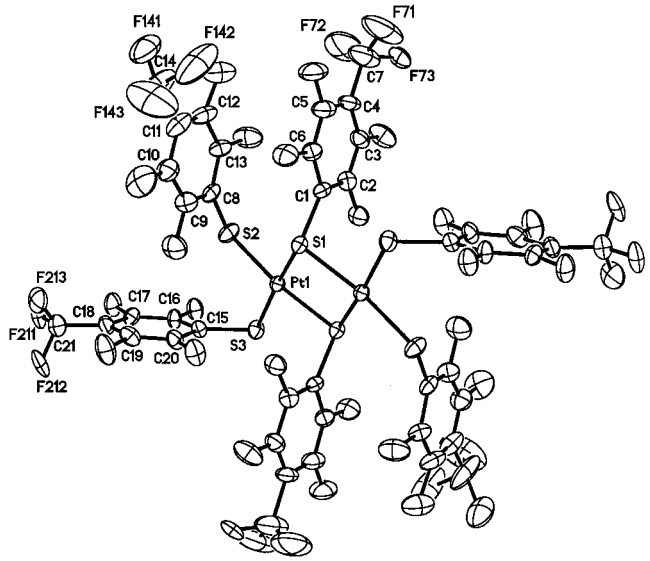

Figure 3. Structure of anion **3b** showing 20% probability displacement ellipsoids. Note the thermal agitation for ligand S3.

Variable-Temperature NMR Studies. Room temperature ^{1}H and ^{19}F NMR data for compounds **1b**, **2b**, and **3b** have been deposited as Supporting Information.

^{195}Pt NMR spectra for compounds **1b**, **2b**, and **3b**, (−3202.6, −3178.8, and −3178.3 ppm, respectively), acquired at room temperature, each show a relatively broad (ca. 2100 Hz at half-height) signal only, suggesting the presence of several species.

The expected magnetic systems for the fluorinated rings C_6F_5, *p*-C_6HF_4, and *p*-$C_6F_4(CF_3)$ can be described as AA′BB′C, AA′BB′X, and AA′BB′X_3, respectively. All three systems share ortho (A = F) and meta (B = F) fluorine nuclei but bear different para substituents, namely, C = F, X = H, and X_3 = CF_3. In each anion **1**−**3** there are two bridging and four terminal ligands and the room temperature ^{19}F NMR spectra of these complexes are therefore expected to include bridge and terminal absorptions—with a 1(bridge):2(terminal) ratio—for each ortho, meta, and para substituent.

The experimental data at room temperature show that bridging ligands give rise to relatively broad absorptions since they are particularly sensitive to variations in the configuration. The lack of definition for these signals precludes an accurate measurement of coupling constants. The terminal ligands, however, give rise to more defined absorptions, and the corresponding coupling constants were measured.

The complexes $[Pt_2(\mu\text{-}SC_6F_5)_2(SC_6F_5)_4]$ **1** and $[Pt_2(\mu\text{-}p\text{-}SC_6F_4(CF_3))_2(p\text{-}SC_6F_4(CF_3))_4]$ **3** belong to the still uncommon family of perfluorinated metal complexes and, as such, the study of their fluxional behavior is confined to the study of ^{19}F nuclei.

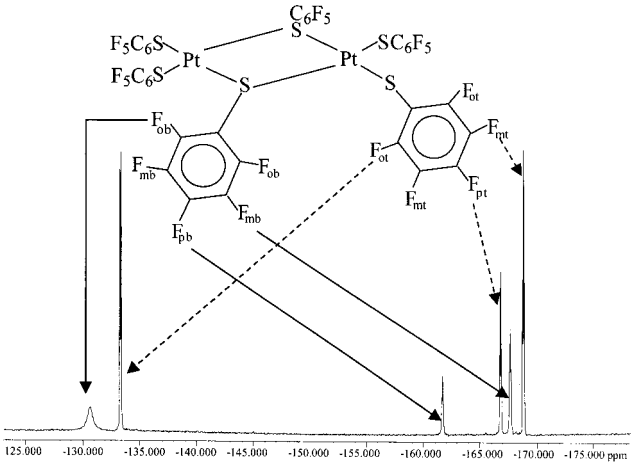

Figure 4. Room temperature ^{19}F NMR spectrum of $(Bu_4N)_2[Pt_2(\mu\text{-}SC_6F_5)_2(SC_6F_5)_4]$ **1b**.

On the other hand, the NMR spectrum of a fluxional molecule depends on the rate of exchange, the difference in resonance frequency of the exchanging species, and the frequency of the observed nucleus within the molecule. For example, in the case reported here, the observed ^{19}F nuclei (ortho and meta) are separated by ca. 10.45 kHz and the resolution of each signal varies considerably. For this reason, the following discussion is focused mainly on the *o*-fluorine region of the ^{19}F NMR spectrum, which shows better definition at all temperatures.

Simulated spectra were obtained using the program gNMR-3.[25] The values of $\Delta G^{\ddagger}_{298}$ for the fluxional processes found were calculated according to the Eyring equation using curve fitting.[26−29]

$(Bu_4N)_2[Pt_2(\mu\text{-}SC_6F_5)_2(SC_6F_5)_4]$ 1b. As shown in Figure 4, the room temperature ^{19}F NMR spectrum of the compound $(Bu_4N)_2[Pt_2(\mu\text{-}SC_6F_5)_2(SC_6F_5)_4]$ exhibits two sets of absorptions: one set with three relatively sharp signals ($\delta = -133.3$, -166.7, and -168.7 ppm; ratio 2:1:2; total intensity = 2) assigned to ortho, para, and meta fluorine atoms of terminal thiolates and a second set with three relatively broad absorptions ($\delta = -130.7$, -167.6, and -161.6 ppm; ratio 2:1:2; total intensity = 1) corresponding to ortho, para, and meta fluorine nuclei of the bridging thiolate groups.

An increase in the temperature of the ^{19}F NMR experiments to 50 °C (see Figure 5) gave rise to sharper signals for both the terminal and bridging thiolate ligands. However, complete definition, particularly regarding the bridging signals, was not reached, and therefore the condition of a fast exchange process is not attained.

As the temperature of the experiments was decreased, the bridge fluorine signals became broader, and at ca. −30 °C the absorption due to the terminal *o*-fluorine nuclei becomes two separate signals, as shown in Figure 5. This phenomenon indicates the presence of syn and anti isomers (relative intensity 1:10), which are in equilibrium through a sulfur inversion process for which a value of $\Delta G^{\ddagger}_{298} = 56.82 \pm 1$ kJ mol^{-1} was estimated. Errors in $\Delta G^{\ddagger}$ were calculated from the standard deviation term $|\sigma(\Delta H^{\ddagger}) - T\sigma(\Delta S^{\ddagger})|$ as described by Binsch and Kessler.[30]

With the exception of the *p*-fluorine nuclei, decreasing the temperature of the NMR experiments caused the broad signals of the bridging thiolate ligands to separate into two pairs of absorptions. At the lowest experimental temperature (−90 °C) the ^{19}F NMR spectra of both syn and anti isomers show 1:1 doublets for the *o*-fluorine nuclei (syn, $\delta = -121.6$, -134.6 ppm, and anti, $\delta = -125.6$, -136.4 ppm), indicating that restricted rotation about the S−C_6F_5 bond makes the *o*-fluorine atoms nonequivalent. At −90 °C the spectrum consists of two overlapping subspectra corresponding to the syn and anti isomers, as shown in Figure 6.

It is worth mentioning at this point that, as noted previously,[11] signals assigned to *p*-fluorine nuclei on rotating rings do not show significant changes in shift nor in signal width upon changing the temperature. Hindered ring rotation around the S−C bond does, however, affect the ortho and meta fluorine

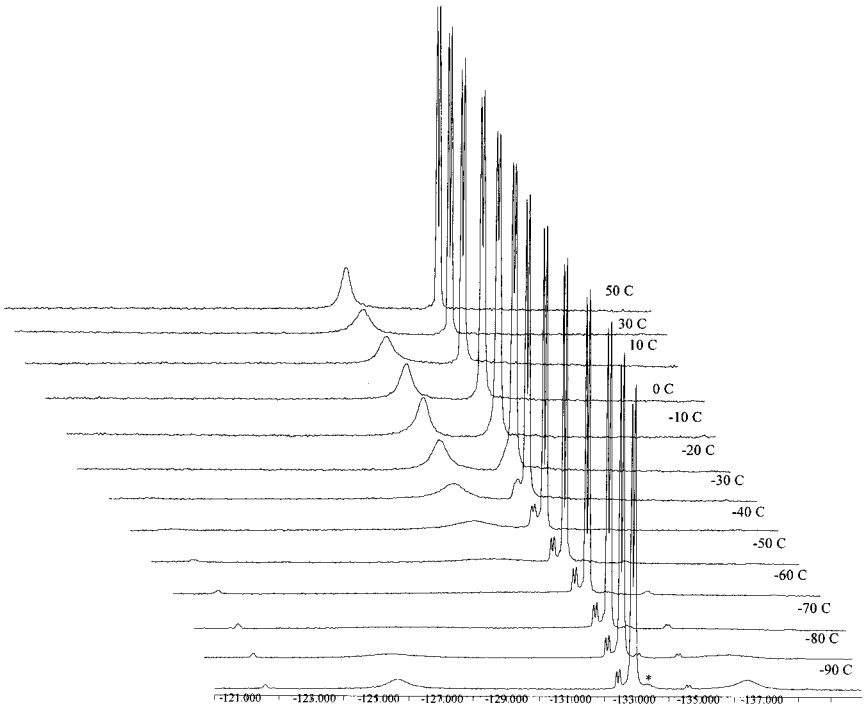

Figure 5. Variable-temperature ^{19}F NMR spectra of $(Bu_4N)_2[Pt_2(\mu\text{-}SC_6F_5)_2(SC_6F_5)_4]$ **1b**.

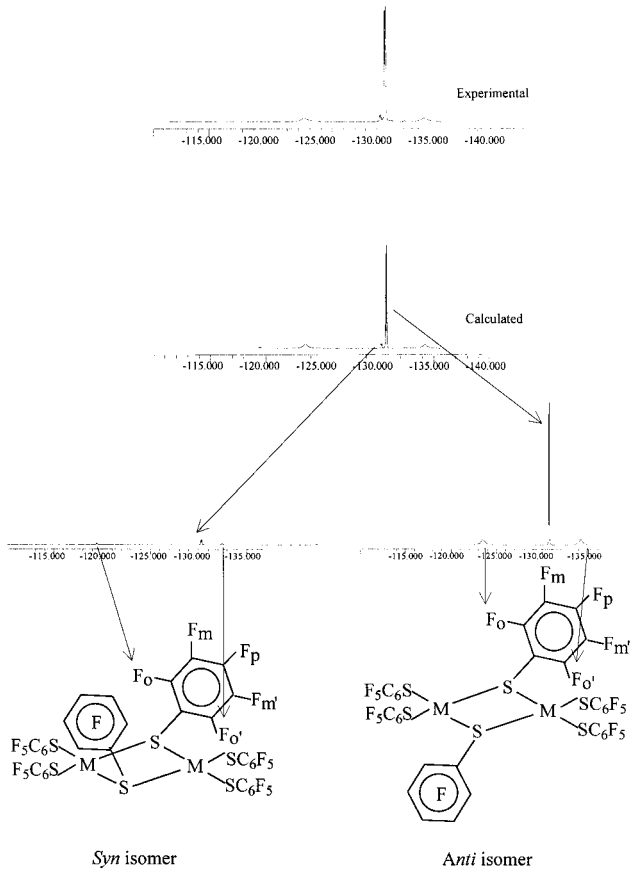

Figure 6. Subspectra in the variable-temperature ^{19}F NMR of $(Bu_4N)_2[Pt_2(\mu\text{-}SC_6F_5)_2(SC_6F_5)_4]$ **1b**, showing syn and anti isomers with frozen rings at the bridging thiolate ligands.

nuclei, which eventually give rise to two different ortho and two distinct meta fluorine signals upon lowering the temperature.

As expected, the energies involved in the carbon−sulfur bond rotation are different for each of the syn and anti isomers. The corresponding calculated activation energies are syn, $\Delta G^{\ddagger}_{298} = 59.87 \pm 0.5$ kJ mol^{-1}, and anti, $\Delta G^{\ddagger}_{298} = 41.85 \pm 0.4$ kJ mol^{-1}.

Molecular modeling strongly suggests that the steric interactions involved in an anti configuration are much less significant than in the syn configuration. This situation implies that the former configuration should be more abundant. On the basis of this assumption, the relative population of isomers, as obtained from the experimental spectrum, should be anti 10:syn 1.

$(Bu_4N)_2[Pt_2(\mu\text{-}p\text{-}SC_6HF_4)_2(p\text{-}SC_6HF_4)_4]$ 2b. The room temperature ^{19}F NMR spectrum of the compound $(Bu_4N)_2[Pt_2(\mu\text{-}p\text{-}SC_6HF_4)_2(p\text{-}SC_6HF_4)_4]$ exhibits two signals ($\delta = -131.7$ and -143.5 ppm; ratio 1:1, total intensity = 2) assigned to the *o*- and *m*-fluorine nuclei of terminal thiolate ligands and two broad signals ($\delta = -128.6$ and -142.1 ppm; ratio 1:1, total intensity = 1) corresponding to *o*- and *m*-fluorine nuclei of the bridging thiolate groups.

As in the cases discussed above, increasing the temperature up to 50 °C gave rise to sharper signals for both the terminal and bridging thiolates, but only the terminal absorptions show an incipient fine structure.

As found for compound **1b**, decreasing the temperature down to −30 °C causes the absorption due to the terminal *o*-fluorine nuclei to split into two signals. Once again this indicates the presence of syn and anti (relative intensity 1:4) isomers that are in equilibrium through a sulfur inversion process, for which $\Delta G^{\ddagger}_{253} = 54.72 \pm 0.4$ kJ mol^{-1}. At lower temperatures the spectra consist of the two overlapping (syn and anti) subspectra described above.

At the lowest experimental temperature (−90 °C), the ^{19}F NMR spectra of both syn and anti isomers show 1:1 doublets for the *o*-fluorine nuclei (syn, $\delta = -121.06$, -132.66 ppm, and anti, $\delta = -124.8$, -133.97 ppm). These data also indicate that rotation about the $S-C_6HF_4$ bond is restricted, a fact that renders the *o*-fluorine atoms nonequivalent.

The calculated activation energies for the restricted carbon−sulfur bond rotation are syn, $\Delta G^{\ddagger}_{298} = 55.53 \pm 0.5$ kJ mol^{-1}, and anti, $\Delta G^{\ddagger}_{298} = 41.41 \pm 0.5$ kJ mol^{-1}.

$(Bu_4N)_2[Pt_2(\mu\text{-}p\text{-}SC_6F_4(CF_3))_2(p\text{-}SC_6F_4(CF_3))_4]$ 3b. The room temperature ^{19}F NMR spectra of compound **3b** show two triplets ($\delta = -55.47$ and -55.04 ppm; relative intensities 1:2), which have been assigned to the fluorine atoms of the *p*-CF_3 groups of the bridging and terminal thiolate ligands, respectively. Furthermore, two sharp signals ($\delta = -130.83$ and -145.91 ppm, ratio 1:1, total intensity 2) have been assigned to ortho and meta fluorine nuclei of the terminal thiolates and two broad signals ($\delta = -127.28$ and -143.67 ppm, ratio 1:1, total intensity 1) assigned to the ortho and meta fluorine nuclei of the bridging thiolate groups.

A decrease in the acquisition temperature to −30 °C causes the absorption due to the terminal *p*-CF_3 groups to split into two signals, which again indicates the presence of syn and anti isomers (relative intensity 1:5). The calculated energy for this sulfur inversion process is $\Delta G^{\ddagger}_{298} = 58.32 \pm 0.7$ kJ mol^{-1}.

At the lowest experimental temperature (−90 °C) the ^{19}F NMR spectra of both syn and anti isomers show 1:1 doublets for the *o*-fluorine nuclei (syn, $\delta = -119.4$, -132.5 ppm, and anti, $\delta = -123.96$, -133.97 ppm), indicating that restricted rotation of the $S-C_6F_4CF_3$ bond renders the *o*-fluorine nuclei nonequivalent. Calculated activation energies for these processes are syn, $\Delta G^{\ddagger}_{298} = 60.00 \pm 0.6$ kJ mol^{-1}, and anti, $\Delta G^{\ddagger}_{298} = 43.18 \pm 0.4$ kJ mol^{-1}.

Acknowledgment. We are grateful to DAGAPA-IN121698 and CONACYT-25108E for their support for this research.

Supporting Information Available: X-ray crystallographic files in CIF format for complexes **1b**, **2b**, and **3b** and a table with ^1H and ^{19}F NMR parameters for complexes **1b**, **2b**, and **3b**. This material is available free of charge via the Internet at http://pubs.acs.org.

IC010437N

(25) Budzelaar, P. H. M. *gNMR-3.6*; Cherwell Scientific Publishing Limited: Oxford, UK, 1995.
(26) Sandström, J. *Dynamic NMR Spectroscopy*; Academic Press: New York, 1982.
(27) Friebolin, H. *Basic One and Two-Dimensional NMR Spectroscopy*; VCH Publishers: New York, 1995.
(28) Abel, E. W.; Bhargava, S. K.; Orrell, K. G. *Prog. Inorg. Chem.* **1984**, *32*, 1−118.
(29) Orrell, K. G. *Coord. Chem. Rev.* **1989**, *96*, 1−48.
(30) Binsch, G.; Kessler, H. *Angew. Chem., Int. Ed. Engl.* **1980**, *19*, 411−428.